

Graph Neural Network Potential for Magnetic Materials

Hongyu Yu,^{a,b} Yang Zhong^{a,b}, Changsong Xu^{a,b}, Xingao Gong,^{a,b} Hongjun Xiang^{a,b,†}

^a*Key Laboratory of Computational Physical Sciences (Ministry of Education), Institute of Computational Physical Sciences, and Department of Physics, Fudan University, Shanghai 200433, China*

^b*Shanghai Qi Zhi Institute, Shanghai 200030, China*

Abstract:

Machine Learning (ML) interatomic potential has shown its great power in condensed matter physics. However, ML interatomic potential for a magnetic system including both structural degrees of freedom and magnetic moments has not been well developed yet. A spin-dependent ML interatomic potential approach based on the crystal graph neural network (GNN) has been developed for any magnetic system. It consists of the Heisenberg edge graph neural network (HEGNN) and spin-distance edge graph neural network (SEGNN). The network captures the Heisenberg coefficient variation between different structures and the fine spin-lattice coupling of high order and multi-body interaction with high accuracy. In the tests, this method perfectly fitted a high-order spin Hamiltonian and two complex spin-lattice Hamiltonian and captured the fine spin-lattice coupling in BiFeO₃. In addition, a disturbed structure of BiFeO₃ with strain was successfully optimized with the trained potential. Our work has expanded the powerful ML GNN potentials to magnetic systems, which paves a new way for large-scale dynamic simulations on spin-lattice coupled systems.

Main text

Machine learning interatomic potentials (MLIPs) have been widely used for material modeling with a balance of speed and accuracy in recent years [1–4]. With the strong expression ability of neural networks, complex interatomic multidimensional energy landscapes can be learned from datasets containing different structures. Compared with *ab initio* calculation, machine learning potentials can significantly reduce the computational cost, leading to feasible simulations of large systems [5–11]. MLIP models are usually built with the kernel-based ML algorithms which use the descriptors of materials as the input and learn the mapping function between the input descriptor and the material's corresponding energy, such as kernel ridge regression (KRR) and gaussian process regression (GPR) methods. The descriptor derived from the atomic positions and the atomic numbers are invariant under uniform translations, rotations, and permutations of identical atoms in materials and greatly influence the performance of the MLIP model. A large variety of descriptors have been developed to encode the material information [12–18]. The smooth overlap of atomic positions [19] (SOAP) and the atom-centered symmetry functions [20,21] (ACSFs) are two of the most used descriptors that characterize the local environments of atoms as the atomic fingerprint. However, most of the descriptor only works for potential without the freedom degrees of atomic magnetic moments. As a result, most MLIP models cannot describe the spin-lattice coupling in magnetic materials. Only very recently, Ivan *et al.* first presented magnetic Moment Tensor Potentials [22] (mMTPs) which add the contributions of collinear magnetic moments on Moment Tensor Potentials (MTPS) to include collinear magnetic degrees of freedom in MLIP. The mMTPS are demonstrated for the prototype magnetic system bcc iron with phonon calculations and molecular dynamics simulations. However, mMTPS can only deal with collinear spin and did not consider the spin-inversion symmetry explicitly, which are instead realized by data augmentation in the model. Marco *et al.* then developed magnetic high dimensional neural network potential (mHDNNP) which modifies the ACSFs to spin-dependent ACSFs (sACSFs) [23]. Same with mMTPS, mHDNNP can only deal with collinear magnetic moments, which holds back the study of noncollinear magnetic states such as spirals, skyrmions, and bimerons. Note that considering noncollinear magnetic states is indispensable for calculating magnetic transition temperature with Monte Carlo simulation and performing spin-molecular dynamics [24,25]. Meanwhile, in a recent

study, Behnam *et al.* point out that both SOAP and ACSFs, the two most commonly used descriptors, fail in treating correctly four-body interactions [26] which leads to a failure of learning the full energy landscape of materials. As a result, MLIP with noncollinear magnetic degrees of freedom is still underdeveloped.

Graph neural network (GNN) as a message-passing deep learning architecture has shown its great power in condensed matter physics. The 3D geometric structure of materials can be described as a connected graph. With the message passing graph neural network, structure representations are learned directly from the input structure using a more natural method without manual construction. Symmetry invariants including translation, rotation, and permutation are naturally included in the graph representations of GNN. Crystal graph neural network (CGNN), as an end-to-end learned natural descriptor for crystal, has been well developed these years [27–35]. A recently proposed Line Graph Neural Network (LGNN) includes the bond angles explicitly and updates the edge features in the graph, such as Dimenet++ [28,29,35]. CGNN has shown outstanding performance in training potential, interpreting materials, predicting properties, and inverse design [27,36–39]. However, to our best knowledge, freedom of degrees of magnetic moments has not been included in CGNN yet.

In this Letter, we present a generalized spin-dependent graph neural network (SGNN) framework for including the noncollinear spin in the CGNN that extends the CGNN to the level of describing the structure and magnetic states. Our SGNN framework includes the Heisenberg edge graph neural network (HEGNN) and the spin-distance edge graph neural network (SEGNN). HEGNN utilizes the updated features of the edges in LGNN which map the variational Heisenberg coefficients between magnetic atoms. As for SEGNN, comparing with edge initialization only with the atomic distance between two atoms in CGNN, both the atomic distance and the dot product of the noncollinear spin between two atoms are applied to initialize the edges in SEGNN. GNN potential with magnetic degrees of freedom can be trained with HEGNN and SEGNN, while HEGNN learns the basic Heisenberg magnetic potential and the complex high-order magnetic potential can be learned by SEGNN.

Spin-dependent graph neural network approach. In this work, we aim to build an approach that includes the noncollinear spin in the crystal graph including HEGNN and SEGNN. Both HEGNN and SEGNN can be used to build the magnetic potential in

ensembles or separately. HEGNN is an expert for describing the simple Heisenberg 2-order magnetic interactions while SEGNN can generally cover both 2-order and higher-order thanks to the message-passing GNN. In principle, SEGNN is powerful enough to include most spin-lattice interactions. Because Heisenberg interactions dominate the magnetic potentials, here HEGNN is introduced to express the Heisenberg interactions. For materials with simple magnetic interaction that can be expressed with the Heisenberg model and the effect of high-order can be neglected, HEGNN is powerful enough to construct the landscape of magnetic potential while SEGNN should be included in the magnetic potential when high-order magnetic interaction is remarkable. As for general magnetic potentials, HEGNN and SEGNN work in ensembles expressed as

$$E^{\text{total}} = E^{\text{HEGNN}}(r, \vec{s}) + E^{\text{SEGNN}}(r, \vec{s}) \quad (1)$$

$$E^{\text{HEGNN}}(r, \vec{s}) = \sum_i h_i^{\text{HEGNN}}(r) + \sum_{i,j} J_{ij}^{\text{HEGNN}}(r) \langle \vec{s}_i, \vec{s}_j \rangle \quad (2)$$

$$E^{\text{SEGNN}}(r, \vec{s}) = \sum_i h_i^{\text{SEGNN}}(r, \vec{s}) \quad (3)$$

where $h_i^{\text{HEGNN}}(r)$ represents HEGNN part of the local atomic energy of atom i and $J_{ij}^{\text{HEGNN}}(r)$ represents the Heisenberg coefficient of the bond of atom i and j which both only relates to the position of the surrounding atoms. $h_i^{\text{SEGNN}}(r, \vec{s})$ represents the SEGNN part of the local atomic energy of atom i which relates to the position and spin vector of the surrounding atoms.

HEGNN. We first introduce the HEGNN based on the Heisenberg model and line graph of crystal. Heisenberg model, as the basic and usually dominant magnetic interaction of materials, is expressed as $H_{HB} = \sum_{i>j} J_{ij}(r) \langle \vec{s}_i, \vec{s}_j \rangle$ where $J_{ij}(r)$ is related to the atomic environment of the bond between two magnetic atoms. However, it's not easy to define the explicit Heisenberg coefficient $J_{ij}(r)$ which is influenced by the relative positions of surrounding atoms. The Heisenberg coefficient is usually

simplified as $J_{ij}(r_{ij})$ with the assumption that it is only affected by the atomic distance between the two magnetic atoms, which ignores the many-body effect. In LGNN, the edges of the graph are updated and can reflect the surrounding atomic information of the magnetic bond. As a result, the updated features of the edges in the line graph are the learned Heisenberg coefficient $J_{ij}(r)$ which includes the information of the neighbor atoms of the magnetic bond. The updated features of the nodes are the learned structure descriptors same as the usual crystal graph. The local magnetic potential of HEGNN can be expressed as $\sum_i E_i^{HEGNN} = \sum_i E_i^{pos}(r) + \sum_{i,j} J_{ij}(r) \langle \vec{s}_i, \vec{s}_j \rangle$ where $E_i^{pos}(r)$, as the traditional structure potential, comes from the learned node feature and $J_{ij}(r)$, as the Heisenberg coefficient, comes from the learned edge feature. We would like to stress that the usual GNN (such as CGCNN) but not LGNN is not applicable in the framework of HEGNN. As the output edge features of GNN, $J_{ij}(r)$, should learn the atomic environments of the bond between atom i and j , the edge should be influenced by the neighbor atoms around the bond. However, in the multigraph of crystal, several edges exist between two nodes. If edges initialization are only related to the bond length while two edges are the same in length but different in directions, the updated edges will remain the same during updates in GNN with only node and edge, which fails in distinguishing these two edges and describing bond's atomic environment. Instead, edge updates in LGNN without this bug. Line graph, as the single graph that exists at most one edge between nodes, describes the atomic environment of the bonds completely. See details of the proof in SM. To be more specific, the cubic perovskite ABO_3 is provided for better intuition. The ideal structure of ABO_3 without distortion and ABO_3 with oxygen octahedral rotation are shown respectively in Fig.3(a) and Fig.3(b). We focus on the bond of intralayer B1-B2 and interlayer B1-B1 in Fig.3. They are the same bond in Fig.3(a) concerning the symmetry but differ in Fig.3(b) because of the oxygen octahedral rotation. In Fig.3(b), B1-O-B1 is still on the same line while B1-O-B2 forms a triangle. As a result, the Heisenberg coefficients of the bond of B1-B2 and B1-B1 are different. However, all Mn atoms in Fig.3(b) are the same and share the same node features. The bond of B1-B2 and B1-B1 have the same length

and also share the same initial edge feature. In general GNN, the edge features of these two different bonds are updated to the same new features as the node features and edge features as the variables are the same which gives the same Heisenberg coefficient. So the usual GNN cannot distinguish these two bonds. In LGNN, as the triplet features are included in the update, the change of the position of the oxygen between two Mn influences the update process. Hence the LGNN gives different Heisenberg coefficients for these two different bonds and distinguishes them. In conclusion, LGNN should be implemented in the framework of HEGNN.

SEGNN. Then, we introduce the SEGNN based on the crystal graph with the spin-distance edge feature. For edge initialization of crystal graph, radial basis functions are usually used such as gaussian expansion [36] and Bessel functions with atomic distance as the only input [28]. We propose the spin-distance edge with the bond information of not only the distance but also the spin product, $\langle \vec{s}_i, \vec{s}_j \rangle$. It could be expressed as

$$e_{ij}^{spin\ distance} = \text{MLP} \left(\text{MLP} \left(rbf(|\vec{r}_{ij}|) \right) \parallel \text{MLP}(\text{Guassian}(\langle \vec{s}_i, \vec{s}_j \rangle)) \right) \quad (4)$$

As the Gaussian basis of distance edge, we first construct spin edge with the Gaussian basis of the value of $\langle \vec{s}_i, \vec{s}_j \rangle$. Then spin edge and distance edge are stacked together as the final spin-distance edge. For bonds with non-magnetic atoms, $\text{MLP}(\text{Guassian}(\langle \vec{s}_i, \vec{s}_j \rangle))$ is treated as a zero array. With spin-distance edges, the spin information is elegantly added to the original crystal graph and any CGNN can describe the magnetic interaction with this modification on the edge initialization process. As only the node features form the output of SEGNN, any GNN can be implemented in the framework of SEGNN to build magnetic potentials.

GNN implementation. Dimenet++ [28,29], as an outstanding line graph neural network for materials, is applied within our SGNN framework and used to build machine learning magnetic atomic potentials for both HEGNN and SEGNN in this work.

Training. We trained the potential by minimizing the squared error loss function. If the forces are provided in the dataset, the loss function is written as

$$L_e = |E - \hat{E}|^2,$$

$$L_f = \frac{1}{n_{\text{atoms}}} \sum_{i=0}^{n_{\text{atoms}}} |F_i - \left(-\frac{\partial E}{\partial R_i}\right)|^2,$$

$$L_{\text{total}} = \rho L_e + L_f,$$

where ρ is a trade-off hyperparameter between loss of energy and force [40]. The choice of ρ influence the performance greatly and should be tuned for different jobs which cost a lot of computational resources [27]. In this work, automatic weighted loss are used, written as

$$l_{\text{aw_total}} = \frac{1}{2\sigma_e^2} L_e + \frac{1}{2\sigma_f^2} L_f + \log(\sigma_e \sigma_f),$$

where $\sigma_{e/f}$ is the parameters that are changing during the training, which shows significant improvement in performance without a heavy job in hyperparameter tuning of the loss coefficients [41]. As a useful loss function for multitask learning, automatic weight loss is first applied in the training of potential to our best knowledge. With more broad applications, we expect it to help with training better MLIP.

Tests of the SGNN framework.

Spin Hamiltonian of an artificial model. We first validate our machine learning potential by constructing a spin Hamiltonian of a fixed structure that only considers spin degrees of freedom. An artificial model is employed with Heisenberg interactions, 4th-order biquadratic interactions, and 4-body 4th-order interactions. This model is intended to describe the spin interactions between magnetic ions that occupy the Al sites of the CuAlO₂-type [42] structure. The model spin Hamiltonian contains both intralayer interactions within the triangular lattice and interlayer couplings:

$$H = \sum_{\langle ij \rangle_n}^{n=1,\dots,5} J_n \mathbf{S}_i \cdot \mathbf{S}_j + \sum_{\langle ij \rangle_n}^{n=1,5,7} K_n (\mathbf{S}_i \cdot \mathbf{S}_j)^2 + \sum_{\langle ijkl \rangle_1} L_1 (\mathbf{S}_i \cdot \mathbf{S}_j)(\mathbf{S}_k \cdot \mathbf{S}_l). \quad (5)$$

See more details of this model in the Supplemental Materials (SM). The dataset of

10,000 fully random spin configurations is generated based on a $4 \times 4 \times 2$ supercell with 96 magnetic sites (*i.e.*, six layers of 4×4 triangular lattices), and their energies are obtained from Eq. (5) as the target. As high-order interactions should be considered, HEGNN and SEGNN are used together for constructing the GNN spin Hamiltonian and they fit the model well shown in Fig. 4(a) with the mean absolute error (MAE, defined as $\frac{\sum |f(x_i) - y_i|}{n}$) as 1.024×10^{-5} meV/site which slightly outperforms the result of the machine learning spin Hamiltonian based on the spin descriptor (1.03×10^{-5} meV/site) [43]. HEGNN and SEGNN can successfully rebuild the energy landscape of a complex spin Hamiltonian.

Two artificial spin-lattice models. To validate our machine learning approach for constructing magnetic potential including both the structural and magnetic degrees of freedom, we employed two complex spin-lattice model potentials. The first is a Heisenberg-type model potential and the second includes higher-order magnetic interactions. Both model potentials are intended to describe the spin-lattice couplings in the ABO_3 perovskite structure with the magnetic B-sites.

The first model potential does not contain high-order spin interactions. It includes interactions up to three-body and second-order including 108 terms that can be expressed as

$$H = \sum_{\langle ij \rangle}^{r < 7\text{\AA}} J_{33}(r_i, r_j, r_k) u_{ijj/k} (\mathbf{S}_i \cdot \mathbf{S}_j) + J_{22}(r_i, r_j, r_k) (\mathbf{S}_i \cdot \mathbf{S}_j) + E_3(r_i, r_j, r_k) + \sum_{\langle ij \rangle}^{r < 7\text{\AA}} J_{23}(r_i, r_j) u_{ijj} (\mathbf{S}_i \cdot \mathbf{S}_j) + J_{22}(r_i, r_j) (\mathbf{S}_i \cdot \mathbf{S}_j) + E_2(r_i, r_j),$$

where J_{ij} indicates the Heisenberg coefficient of i -body and j^{th} -order which is all set as 0.1 eV while other coefficients of terms only related with positions are 1 eV. This spin-lattice model potential is a complex Heisenberg model which not consider high-order magnetic interaction. 2416 data with different distortions and spin configurations are generated. Data are randomly separated for training, validating, and testing with the ratio of 80%, 10%, and 10% respectively. As the first model only contains Heisenberg

interactions, only HEGNN is used to train and perform well shown in Fig.4(d) with the MAE as 5.04 meV/site. We also compare the performance of ensembling HEGNN and SEGNN which does not achieve a better result with the MAE as 5.57 meV/site. It can be concluded that HEGNN can learn the Heisenberg coefficient well, and HEGNN is powerful enough to learn the Heisenberg-type magnetic potential.

The second model potential contains fourth-order spin interactions. It includes interactions up to three-body and fourth-order including 274 terms that can be expressed as

$$\begin{aligned}
H = & \sum_{\substack{r < 5.71 \text{ \AA} \\ \langle ijk \rangle_r}} J_{34}(r_i, r_j, r_k) u_{i/j/k} u_{i/j/k} (\mathbf{S}_i \cdot \mathbf{S}_j) + J_{33}(r_i, r_j, r_k) u_{i/j/k} (\mathbf{S}_i \cdot \mathbf{S}_j) J_{32}(r_i, r_j, r_k) (\mathbf{S}_i \cdot \mathbf{S}_j) + \\
& + L(r_i, r_j, r_k) (\mathbf{S}_i \cdot \mathbf{S}_j) (\mathbf{S}_i \cdot \mathbf{S}_k) + E_3(r_i, r_j, r_k) \\
& \sum_{\substack{r < 5.71 \text{ \AA} \\ \langle ij \rangle_r}} J_{24}(r_i, r_j) u_{i/j} u_{i/j} (\mathbf{S}_i \cdot \mathbf{S}_j) + J_{23}(r_i, r_j) u_{i/j} (\mathbf{S}_i \cdot \mathbf{S}_j) + J_{22}(r_i, r_j) (\mathbf{S}_i \cdot \mathbf{S}_j) + \\
& E_2(r_i, r_j),
\end{aligned}$$

where coefficients are set the same with the first model that spin-related coefficients as 0.1 eV and others as 1 eV. This model potential includes not only Heisenberg-type terms but also fourth-order terms $L(r_i, r_j, r_k) (\mathbf{S}_i \cdot \mathbf{S}_j) (\mathbf{S}_i \cdot \mathbf{S}_k)$, which is not able to be learned by HEGNN solely. 3611 data are generated and split the same as the first model. On account of high-order interactions are included in the second model, HEGNN solely can not learn it and SEGNN should be used. We first only use SEGNN to fit, which gives a relatively good result shown in Fig.4(b) with an MAE of 0.0298 eV. Then HEGNN and SEGNN are used together to fit, which gives a better result shown in Fig.4(e) with MAE as 0.0233 eV. HEGNN, as an expert in learning Heisenberg interactions, helps to achieve better accuracy.

Application-Multiferroic BiFeO_3 . BiFeO_3 (BFO) is a room-temperature multiferroic materials. Spin-lattice model potentials are traditionally used to understand the spin-lattice coupling in multiferroic materials such as BFO according to the symmetry of the system [44]. However, it's usually hard to determine the terms and

related coefficients to build the potential. We apply our SGNN to build magnetic potential for BFO and optimize the disturbed structure of BFO with the potential. As for the dataset, 4012 random spin configurations within a $4 \times 4 \times 4$ supercell BFO, which contains 64 Fe and structures are randomly selected from several molecular dynamics, and their energies are computed with DFT (see Methods in SM). Again, 80% of the data are used for training, 10% for validating, and 10% for testing. Both energies and forces are provided as the target and automatic weighed loss is used as the loss function. We first train with HEGNN alone. It achieves high accuracy with MAE as 0.0495 meV/site on the energy and 3.43 meV/Å on the force shown in Fig. 4(c) and Fig. 4(f). Then we train with HEGNN and SEGNN together. The assembling of SEGNN does not contribute to better accuracy and only gives a similar MAE of 0.0501 meV/site on the energy and 3.54 meV/Å on the force. HEGNN solely can provide an accurate magnetic potential just as the first spin-lattice model considering Heisenberg-type interaction. In conclusion, BFO is a Heisenberg-type magnetic material obviously.

To prove the validity of the potential, we optimize a disturbed structure of BFO with G-type AFM magnetic configuration with the HEGNN potential and compare the result with DFT. Displacements of 0.2 Å in random direction are applied on each atom of a small supercell with 4 Fe and 1% strain is applied on the cell. The positions of the atoms and the cell are optimized together with the HEGNN potential and the Broyden, Fletcher, Goldfarb, and Shanno (BFGS) algorithm [45] that implemented in Atomic Simulation Environment (ASE) package [46]. As for validation, the same structure is optimized by DFT with the conjugate gradient algorithm in VASP. We evaluate the optimization performance by matching the optimized structure of the HEGNN potential with the BFGS algorithm and VASP. We use StructureMatcher from pymatgen [47], which gives the average root mean square (RMS) displacement between two structures as 0.00389 Å. The structure optimized by HEGNN is also calculated by DFT to check whether it's stable. The average force on atoms is 5 meV/Å and the stress on the cell is $\sigma_{xx} = 8.91 \text{ meV}/\text{Å}^3$, $\sigma_{yy} = 9.47 \text{ meV}/\text{Å}^3$, $\sigma_{zz} = 10.33 \text{ meV}/\text{Å}^3$, $\sigma_{xy} = 0.362 \text{ meV}/\text{Å}$, $\sigma_{yz} = 0.242 \text{ meV}/\text{Å}^3$, $\sigma_{zx} = 0.381 \text{ meV}/\text{Å}^3$, which is quite small. It proves that the optimization is successful and validate the magnetic potential.

In summary, we develop a spin-dependent graph neural network framework to construct the potential including both structural degrees of freedom and noncollinear magnetic moments. Such a framework involves a Heisenberg edge graph and spin-distance edge graph and adopts the graph neural network to describe the complex spin interactions of any form. The framework provides a reliable energy landscape for an artificial high-order spin Hamiltonian, two artificial complex spin-lattice models, and BiFeO₃. The potential successfully optimizes the disturbed structure of BiFeO₃. To consider the spin-orbital coupling, HEGNN can be expanded into regarding DM interaction or other complicated interaction utilizing the edge features. As the presently developed framework could convert existing crystal graph potential into magnetic potential which is important for magnetism, we expect that our framework may find wide use in the study of magnetism.

Acknowledgments. The work at Fudan is supported by NSFC (11825403, 11991061).

† hxiang@fudan.edu.cn

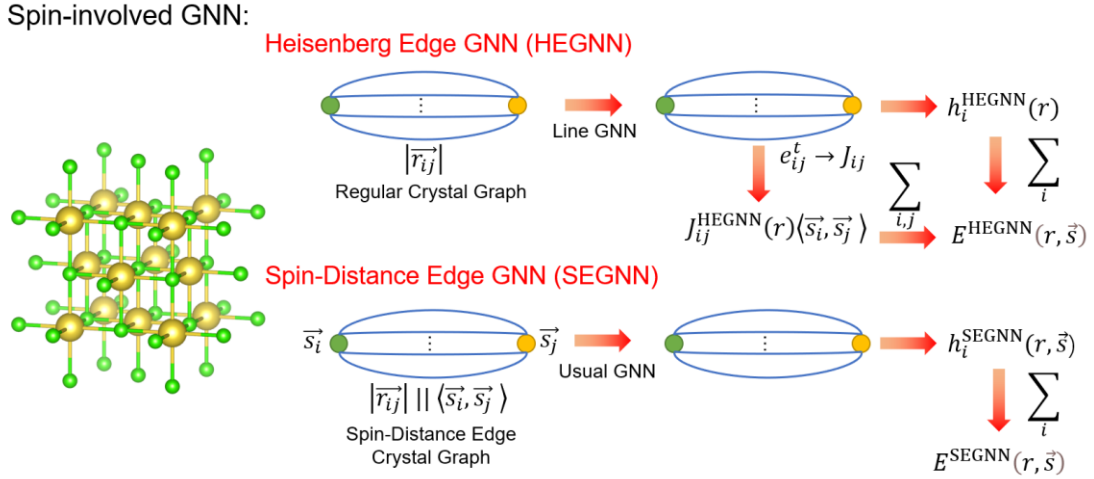


Figure 1. Illustration of the SGNN including HEGNN and SEGNN. HEGNN utilizes the updated edge feature of Line GNN as the Heisenberg coefficients. SEGNN initializes the edge with the dot product of the spin vector and bond length.

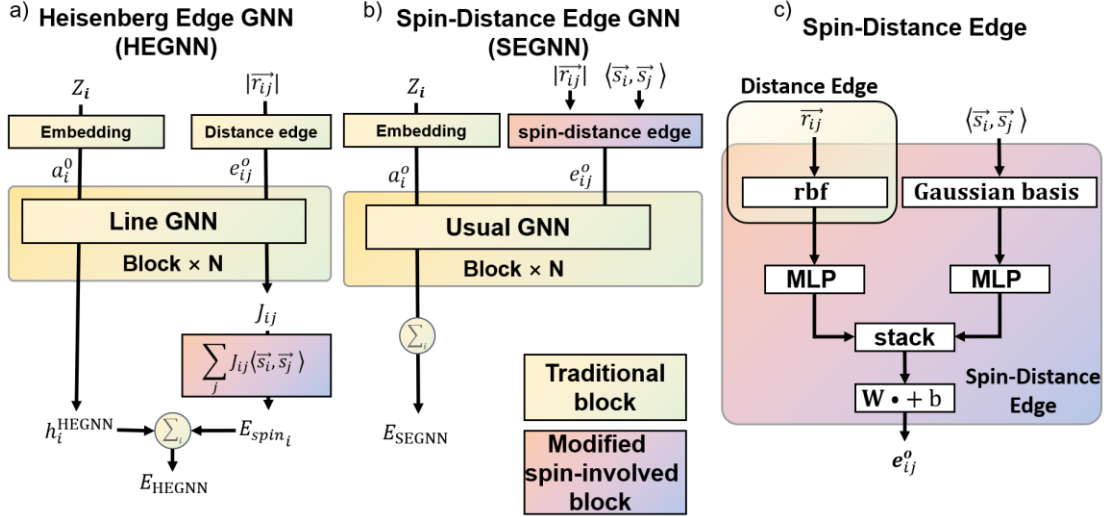


Figure 2. The architecture of our SGNN framework whose modifications on general GNN are highlighted with pink block. The traditional blocks are inherited from the original GNN for materials. a) HEGNN utilizes the edge feature in Line GNN. With the updated edge in Line GNN, HEGNN predicts the Heisenberg coefficients with the final edge and form a Heisenberg-based magnetic potential. b) Spin-distance edge is introduced in SEGNN. Not only the distance of the bond but also the dot product of the spin vector of the two atoms on the bond are utilized featuring the spin-distance edge. c) The framework of implementing the spin-distance edge. Both the distance and spin product are first featured by the expansion function and an MLP (Multilayer Perceptron). Then they are stacked together and featured further by a layer.

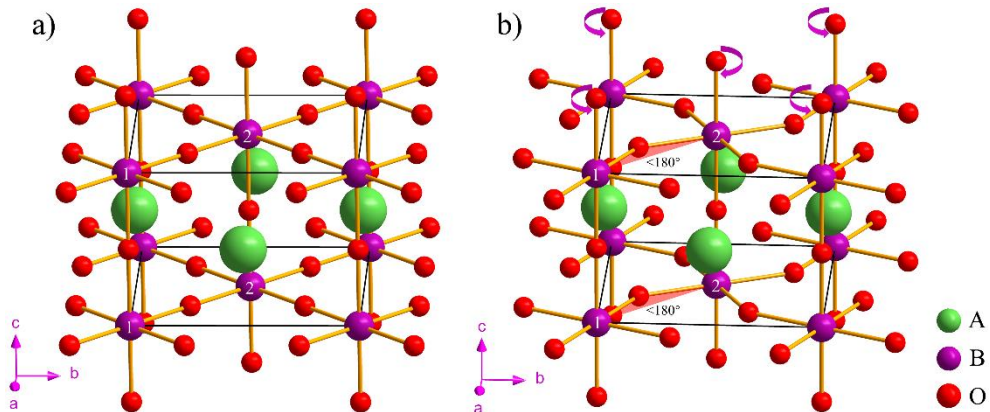


Figure 3. a) Cubic perovskite structure of ABO_3 . b) The distorted perovskite structure of ABO_3 whose oxygen octahedra are rotated along $[001]$ direction. B1-B1 pairs and B1-B2 pairs have the same interatomic distance but different Heisenberg coefficients

because the oxygen octahedral rotation changes the bond environment.

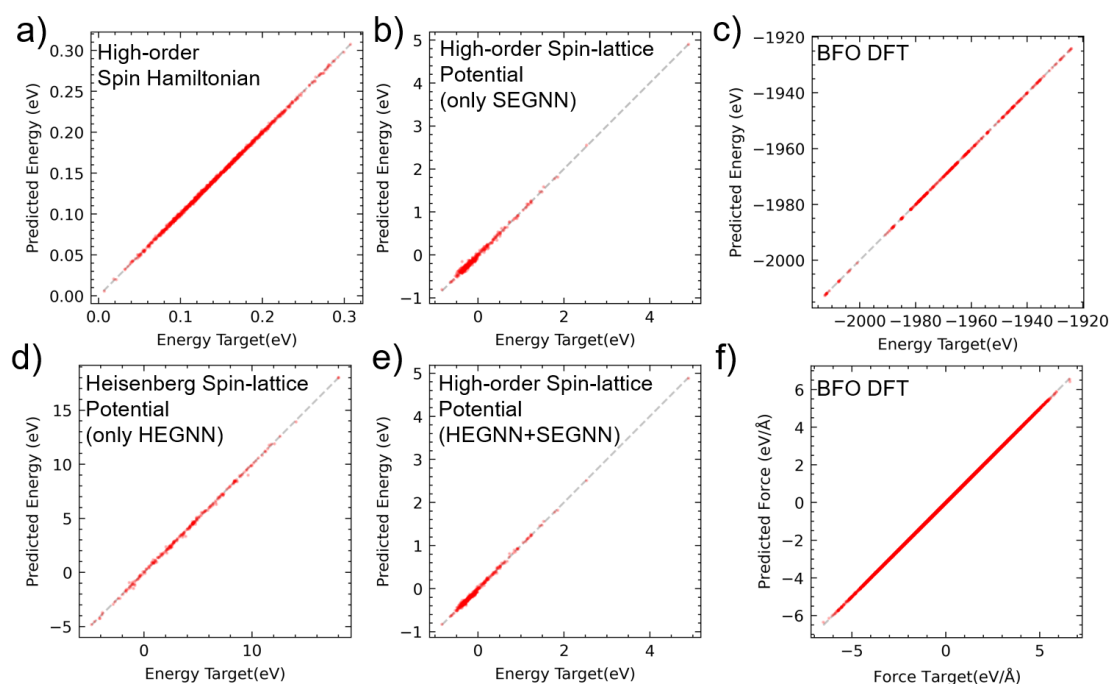


Figure 4. The prediction results of SGNN on the energy of the model test datasets and energy and force of the BFO DFT test datasets.

Reference

- [1] G. R. Schleder, A. C. M. Padilha, C. M. Acosta, M. Costa, and A. Fazzio, *From DFT to Machine Learning: Recent Approaches to Materials Science—a Review*, J. Phys. Mater. **2**, 032001 (2019).
- [2] G. Carleo, I. Cirac, K. Cranmer, L. Daudet, M. Schuld, N. Tishby, L. Vogt-Maranto, and L. Zdeborová, *Machine Learning and the Physical Sciences*, Rev. Mod. Phys. **91**, 045002 (2019).
- [3] A. Agrawal and A. Choudhary, *Perspective: Materials Informatics and Big Data: Realization of the “Fourth Paradigm” of Science in Materials Science*, APL Mater. **4**, 053208 (2016).
- [4] M. Pinheiro, F. Ge, N. Ferré, P. O. Dral, and M. Barbatti, *Choosing the Right Molecular Machine Learning Potential*, Chem. Sci. **12**, 14396 (2021).
- [5] L. Hu, B. Huang, and F. Liu, *Atomistic Mechanism Underlying the Si(111)-(7×7) Surface Reconstruction Revealed by Artificial Neural-Network Potential*, Phys. Rev. Lett. **126**, 176101 (2021).
- [6] A. Krishnamoorthy, K. Nomura, N. Baradwaj, K. Shimamura, P. Rajak, A. Mishra, S. Fukushima, F. Shimojo, R. Kalia, A. Nakano, and P. Vashishta, *Dielectric Constant of Liquid Water Determined with Neural Network Quantum Molecular Dynamics*, Phys. Rev. Lett. **126**, 216403 (2021).
- [7] Z. Li, J. R. Kermode, and A. De Vita, *Molecular Dynamics with On-the-Fly Machine*

- Learning of Quantum-Mechanical Forces*, Phys. Rev. Lett. **114**, 096405 (2015).
- [8] R. Jinnouchi, F. Karsai, and G. Kresse, *On-the-Fly Machine Learning Force Field Generation: Application to Melting Points*, Phys. Rev. B **100**, 014105 (2019).
- [9] H. Suwa, J. S. Smith, N. Lubbers, C. D. Batista, G.-W. Chern, and K. Barros, *Machine Learning for Molecular Dynamics with Strongly Correlated Electrons*, Phys. Rev. B **99**, 161107 (2019).
- [10] Z. Guo, D. Lu, Y. Yan, S. Hu, R. Liu, G. Tan, N. Sun, W. Jiang, L. Liu, Y. Chen, L. Zhang, M. Chen, H. Wang, and W. Jia, *Extending the Limit of Molecular Dynamics with Ab Initio Accuracy to 10 Billion Atoms*, ArXiv220101446 Cs (2022).
- [11] D. Lu, H. Wang, M. Chen, L. Lin, R. Car, W. E, W. Jia, and L. Zhang, *86 PFLOPS Deep Potential Molecular Dynamics Simulation of 100 Million Atoms with Ab Initio Accuracy*, Comput. Phys. Commun. **259**, 107624 (2021).
- [12] L. Himanen, M. O. J. Jäger, E. V. Morooka, F. Federici Canova, Y. S. Ranawat, D. Z. Gao, P. Rinke, and A. S. Foster, *Dscribe: Library of Descriptors for Machine Learning in Materials Science*, Comput. Phys. Commun. **247**, 106949 (2020).
- [13] J. Liu, W. Luo, L. Wang, J. Zhang, X. Fu, and J. Luo, *Toward Excellence of Electrocatalyst Design by Emerging Descriptor-Oriented Machine Learning*, Adv. Funct. Mater. 2110748 (2022).
- [14] O. Isayev, C. Oses, C. Toher, E. Gossett, S. Curtarolo, and A. Tropsha, *Universal Fragment Descriptors for Predicting Properties of Inorganic Crystals*, Nat. Commun. **8**, 1 (2017).
- [15] H. Huo and M. Rupp, *Unified Representation of Molecules and Crystals for Machine Learning*, ArXiv170406439 Cond-Mat Physicsphysics (2018).
- [16] J. S. Smith, O. Isayev, and A. E. Roitberg, *ANI-1: An Extensible Neural Network Potential with DFT Accuracy at Force Field Computational Cost*, Chem. Sci. **8**, 3192 (2017).
- [17] J. Behler, *Atom-Centered Symmetry Functions for Constructing High-Dimensional Neural Network Potentials*, J. Chem. Phys. **134**, 074106 (2011).
- [18] L. Zhang, J. Han, H. Wang, W. A. Saidi, R. Car, and W. E, *End-to-End Symmetry Preserving Inter-Atomic Potential Energy Model for Finite and Extended Systems*, ArXiv180509003 Cond-Mat Physicsphysics (2018).
- [19] A. P. Bartók, R. Kondor, and G. Csányi, *On Representing Chemical Environments*, Phys. Rev. B **87**, 184115 (2013).
- [20] J. Behler, *Atom-Centered Symmetry Functions for Constructing High-Dimensional Neural Network Potentials*, J. Chem. Phys. **134**, 074106 (2011).
- [21] J. Behler and M. Parrinello, *Generalized Neural-Network Representation of High-Dimensional Potential-Energy Surfaces*, Phys. Rev. Lett. **98**, 146401 (2007).
- [22] I. Novikov, B. Grabowski, F. Körmann, and A. Shapeev, *Magnetic Moment Tensor Potentials for Collinear Spin-Polarized Materials Reproduce Different Magnetic States of Bcc Fe*, Npj Comput. Mater. **8**, 1 (2022).
- [23] M. Eckhoff and J. Behler, *High-Dimensional Neural Network Potentials for Magnetic Systems Using Spin-Dependent Atom-Centered Symmetry Functions*, Npj Comput. Mater. **7**, 1 (2021).
- [24] J. Tranchida, S. J. Plimpton, P. Thibaudeau, and A. P. Thompson, *Massively Parallel Symplectic Algorithm for Coupled Magnetic Spin Dynamics and Molecular Dynamics*, J. Comput. Phys. **372**, 406 (2018).

- [25] K. Hukushima and K. Nemoto, *Exchange Monte Carlo Method and Application to Spin Glass Simulations*, J. Phys. Soc. Jpn. **65**, 1604 (1996).
- [26] B. Parsaeifard and S. Goedecker, *Manifolds of Quasi-Constant SOAP and ACSF Fingerprints and the Resulting Failure to Machine Learn Four-Body Interactions*, J. Chem. Phys. **156**, 034302 (2022).
- [27] K. T. Schütt, H. E. Sauceda, P.-J. Kindermans, A. Tkatchenko, and K.-R. Müller, *SchNet – A Deep Learning Architecture for Molecules and Materials*, J. Chem. Phys. **148**, 241722 (2018).
- [28] J. Klicpera, J. Groß, and S. Günnemann, *Directional Message Passing for Molecular Graphs*, ArXiv200303123 Phys. Stat (2020).
- [29] J. Klicpera, S. Giri, J. T. Margraf, and S. Günnemann, *Fast and Uncertainty-Aware Directional Message Passing for Non-Equilibrium Molecules*, ArXiv201114115 Phys. (2020).
- [30] J. Klicpera, F. Becker, and S. Günnemann, *GemNet: Universal Directional Graph Neural Networks for Molecules*, ArXiv210608903 Phys. Stat (2021).
- [31] J. Cheng, C. Zhang, and L. Dong, *A Geometric-Information-Enhanced Crystal Graph Network for Predicting Properties of Materials*, Commun. Mater. **2**, 1 (2021).
- [32] Hu J., Zhao Y., Yang W., Song Y., Siriwardane E. M., Li Y., and Dong R., *AlphaCrystal: Contact map based crystal structure prediction using deep learning*, (2021).
- [33] C. Chen, W. Ye, Y. Zuo, C. Zheng, and S. P. Ong, *Graph Networks as a Universal Machine Learning Framework for Molecules and Crystals*, Chem. Mater. **31**, 3564 (2019).
- [34] J. Schmidt, L. Pettersson, C. Verdozzi, S. Botti, and M. A. L. Marques, *Crystal Graph Attention Networks for the Prediction of Stable Materials*, Sci. Adv. **7**, eabi7948 (n.d.).
- [35] K. Choudhary and B. DeCost, *Atomistic Line Graph Neural Network for Improved Materials Property Predictions*, Npj Comput. Mater. **7**, 1 (2021).
- [36] T. Xie and J. C. Grossman, *Crystal Graph Convolutional Neural Networks for an Accurate and Interpretable Prediction of Material Properties*, Phys. Rev. Lett. **120**, 145301 (2018).
- [37] Q. Wang and L. Zhang, *Inverse Design of Glass Structure with Deep Graph Neural Networks*, ArXiv210406632 Cond-Mat (2021).
- [38] T. Xie, X. Fu, O.-E. Ganea, R. Barzilay, and T. Jaakkola, *Crystal Diffusion Variational Autoencoder for Periodic Material Generation*, ArXiv211006197 Cond-Mat Physicsphysics (2021).
- [39] Z. Ren, J. Noh, S. Tian, F. Oviedo, G. Xing, Q. Liang, A. Aberle, Y. Liu, Q. Li, S. Jayavelu, K. Hippalgaonkar, Y. Jung, and T. Buonassisi, *Inverse Design of Crystals Using Generalized Invertible Crystallographic Representation*, ArXiv200507609 Cond-Mat Physicsphysics (2020).
- [40] A. Pukrittayakamee, M. Malshe, M. Hagan, L. M. Raff, R. Narulkar, S. Bukkapatnum, and R. Komanduri, *Simultaneous Fitting of a Potential-Energy Surface and Its Corresponding Force Fields Using Feedforward Neural Networks*, J. Chem. Phys. **130**, 134101 (2009).
- [41] A. Kendall, Y. Gal, and R. Cipolla, *Multi-Task Learning Using Uncertainty to Weigh Losses for Scene Geometry and Semantics*, ArXiv170507115 Cs (2018).
- [42] T. Ishiguro, A. Kitazawa, N. Mizutani, and M. Kato, *Single-Crystal Growth and Crystal Structure Refinement of CuAlO₂*, J. Solid State Chem. **40**, 170 (1981).
- [43] H. Yu, C. Xu, F. Lou, L. Bellaiche, Z. Hu, X. Gong, and H. Xiang, *Complex Spin Hamiltonian Represented by Artificial Neural Network*, ArXiv211000724 Cond-Mat (2021).
- [44] J. Li, J. Feng, P. Wang, E. Kan, and H. Xiang, *Nature of Spin-Lattice Coupling in Two-Dimensional CrI₃ and CrGeTe₃*, Sci. China Phys. Mech. Astron. **64**, 286811 (2021).

- [45] J. E. Dennis and R. B. Schnable, *Numerical Methods for Unconstrained Optimization and Nonlinear Equations* (1983).
- [46] A. H. Larsen, J. J. Mortensen, J. Blomqvist, I. E. Castelli, R. Christensen, M. Du\lak, J. Friis, M. N. Groves, B. Hammer, C. Hargus, E. D. Hermes, P. C. Jennings, P. B. Jensen, J. Kermode, J. R. Kitchin, E. L. Kolsbjerg, J. Kubal, K. Kaasbjerg, S. Lysgaard, J. B. Maronsson, T. Maxson, T. Olsen, L. Pastewka, A. Peterson, C. Rostgaard, J. Schiøtz, O. Schütt, M. Strange, K. S. Thygesen, T. Vegge, L. Vilhelmsen, M. Walter, Z. Zeng, and K. W. Jacobsen, *The Atomic Simulation Environment—a Python Library for Working with Atoms*, *J. Phys. Condens. Matter* **29**, 273002 (2017).
- [47] S. P. Ong, W. D. Richards, A. Jain, G. Hautier, M. Kocher, S. Cholia, D. Gunter, V. L. Chevrier, K. A. Persson, and G. Ceder, *Python Materials Genomics (Pymatgen): A Robust, Open-Source Python Library for Materials Analysis*, *Comput. Mater. Sci.* **68**, 314 (2013).